Convective transport in the scrape-off-layer

by non-thermalized spinning blobs

J. R. Myra, D. A. D'Ippolito

Lodestar Research Corp., Boulder, CO

S. I. Krasheninnikov, and G. Q. Yu,

University of California at San Diego, La Jolla, CA

Convective transport in the scrape-off-layer

by non-thermalized spinning blobs

J. R. Myra, D. A. D'Ippolito

Lodestar Research Corp., 2400 Central Ave. P-5, Boulder, Colorado 80301

S. I. Krasheninnikov, and G. Q. Yu,

University of California at San Diego, La Jolla, CA 92093

In this paper, two-dimensional blob models of convective transport in the scrape-off-layer (SOL) are generalized to include the internal temperature profile of the blob. This generalization provides a mechanism for blob internal spin and enables consideration of SOL energy transport. Solutions with aligned density and temperature contours satisfy the resulting "hot blob" equations and are considered here. It is shown that spin increases blob coherence, prevents the formation of extended radial streamers or fingers, reduces the radial convection velocity due to mixing and mitigation of the curvature-induced charge polarization, and provides a new mechanism for poloidal motion of the blob. Additionally, spinning blobs are shown to survive as coherent objects in the presence of weak externally sheared flows, and have blob speeds that depend on the sign of the spin relative to the external sheared flow. The work provides strong motivation for investigating the physics of parallel disconnected blobs, and the relationship of spin and disconnection physics to ELM propagation and the density limit.

PACS: 52.25.Fi, 52.35.Ra, 52.55.Dy, 52.55.Fa

I. Introduction

There is a growing recognition of the importance of convective transport in the scrape-off-layer (SOL) of tokamaks and other magnetic confinement devices. Convective processes have been suggested as an explanation for the observed flattening of the plasma density profile in the far SOL,[1] and two-dimensional imaging, as well as probe data, have observed intermittency, and coherent objects which may be responsible for the non-diffusive component of the transport.[2-5] Edge transport analysis has revealed a strong convective component to the observed radial flux.[6] Theoretically, recent investigations have shown the existence of localized coherent "blobs", "fingers", and "fronts" or "streamers" of density that are convected radially outward (i.e. in the direction of the major radius, R) in tokamak geometry by the magnetic curvature and grad-B drifts.[7-11] Because the electrons and ions in a local blob of density experience opposite curvature and grad-B drifts, charge polarization results. In tokamak geometry, the resulting internal blob electric field is poloidal for a blob at the outboard midplane and results in a net outward drift of the blob. This mechanism is analogous to the drift of the localized density enhancement from an injected pellet.[12] Blobs are so named because of their structure in the two-dimensional plane perpendicular to the magnetic field B, and it should be noted that in three dimensions they are filamentary structures, elongated along B. A short review of recent theoretical developments in blob physics is given in Ref. 13.

Previous theoretical blob models have mainly focused on density transport relevant to the far SOL. Parallel loss of excess electron temperature results in thermalization of the blob's electron temperature, T_e, with the ambient background plasma in a time scale $\tau_{E\parallel}$. For times $t > \tau_{E\parallel}$ the "thermalized" blob, considered in detail previously, can transport density but not temperature. The enhanced particle transport to the wall from thermalized blob models provides a theoretical framework for understanding experimental regimes dominated by main chamber recycling.[1] To obtain a more complete understanding of both heat and particle transport in a tokamak it is necessary to consider blobs which carry excess temperature as well as density. This class of models, treated in the present paper, can potentially yield insights into the propagation of hot plasma ejected by phenomena such as edge localized modes (ELMs). An important goal of tokamak edge physics is to understand, and ultimately mitigate or control, the deposition of heat on the divertor plates. This requires an understanding of the importance of perpendicular energy transport relative to the parallel channel. In extreme cases where perpendicular energy transport is sufficiently rapid, it is possible that the divertor may be "short-circuited", with the result that energy would flow primarily radially into the wall or other hardware in the SOL. To assess the conditions under which this is possible, theoretical mechanisms for convective heat transport and estimates of the convective velocity are necessary. That is the subject of the present paper. Although our

present interest is primarily in understanding tokamaks, it will be apparent that many of the concepts apply to the SOL of magnetically confined plasmas in general.

The main new theme explored in this paper is the consequences of a hot blob having an internal electron temperature profile, $T(r)$. For brevity we will call this the "hot" blob case, to distinguish it from the "thermalized" blob case considered previously where $T(r)$ = constant. When the blob is connected to end sheaths along the magnetic field lines, the internal blob temperature profile implies an internal electrostatic potential profile $\Phi(r) \sim 3\,T(r)$ and hence an internal $v_\theta = \partial\Phi/\partial r$ or rotation. We will refer to this internal rotation as spin (to keep it distinct from background plasma rotation).

As demonstrated in this paper, spin influences the net convection velocity of blobs. The curvature-induced drift mechanism attempts to charge polarize the blobs. Spin rotates the separated charges to different angles with respect to the blob center and ultimately mixes them, resulting in mitigation of the charge-polarization mechanism. It slows the blob's convection velocity in x, stalling it in extreme cases, and in intermediate cases gives a mechanism for blob motion in y. Here x and y are a local coordinate system with $\mathbf{e}_x = \mathbf{R}/R$ (tokamak radial) and $\mathbf{e}_y = \mathbf{b} \times \mathbf{e}_x$ (tokamak poloidal) where $\mathbf{b} = \mathbf{B}/B$. Thus, hot blobs that are sheath-connected and hence spinning are not as effective at either energy or particle transport as non-spinning blobs. Other consequences of spin related to density convection will also be investigated.

The plan of our paper is as follows. In Sec. II model equations for investigating hot blob transport will be presented. In Sec. III both numerical and analytical results from these models will be presented. Our conclusions are given in Sec. IV.

II. Model Equations

A minimal set of equations for understanding convective transport of hot blobs consists of the vorticity equation for the electrostatic potential and continuity equations for the plasma density, n, and electron temperature, T. For simplicity we work in the cold ion limit. Normalizing time to the inverse of the ion cyclotron frequency $\Omega_i = ZeB/m_ic$, space to a reference ion Larmor radius $\rho_s = c_s/\Omega$, where $c_s^2 = T_{e0}/m_i$ is the sound speed based on a reference temperature T_{e0}, T to T_{e0}, and n to a reference density, the fundamental equations take the form[8]

$$\frac{d}{dt}\nabla^2\Phi = \frac{\alpha}{T^{1/2}}(\Phi - \Phi_B) - \frac{\beta}{n}\frac{\partial(nT)}{\partial y} - \nu\nabla^2\Phi \tag{1}$$

$$\frac{dn}{dt} = 0 \tag{2}$$

$$\frac{dT}{dt} = 0 \tag{3}$$

3

where

$$\frac{d}{dt} = \frac{\partial}{\partial t} + \mathbf{v} \cdot \nabla \tag{4}$$

$$\mathbf{v} = \mathbf{b} \times \nabla \Phi \tag{5}$$

with sheath parameter $\alpha = 2\rho_s/L_\parallel$ where $L_\parallel$ is the parallel connection length to the sheaths, curvature parameter $\beta = 2\rho_s/R$ and Bohm sheath potential $\Phi_B = \Phi_{B0}T$ where typically $\Phi_{B0} \sim 3$. In Eq. (1) we have made the usual "Boussinesque" approximation $\nabla \cdot (n\ d/dt\ \nabla \Phi) \rightarrow n\ d/dt\ \nabla^2 \Phi$ and divided through by n. The final term in Eq. (1) is regarded here as a phenomenological vorticity damping term. A term of this form can be used to model Alfvén wave damping,[14] parallel plasma viscosity or neutral friction. Parallel energy loss is neglected in Eq. (3), under the assumption that $\tau_c < \tau_{E\parallel}$ where τ_c is a convective time scale of interest, to be defined subsequently. In the opposite limit, $\tau_c > \tau_{E\parallel}$, the blob will quickly thermalize to the background temperature.

Several limiting cases will be useful in the next section to elucidate the behavior of different terms and physical mechanisms. The "thermalized blob equations" result from taking T = constant, which trivially solve Eq. (3). Since Φ_B is then just a constant potential, it may be set to zero, leaving Eqs. (1) and (2) which are the equations studied in Refs. 7 and 8.

For future convenience, we also define two subsidiary forms of the vorticity equation. The first is the dissipative limit $\nu \gg d/dt$

$$(1 - a_s^2 \nabla^2)\Phi = \Phi_B + \frac{qT^{1/2}}{n}\frac{\partial(nT)}{\partial y} \tag{6}$$

where $a_s^2 \equiv \nu T^{1/2}/\alpha$ and $q \equiv \beta/\alpha = L_\parallel/R$. The second is the hydrodynamic, thermalized blob case with T = 1 and $\nu \ll d/dt$.

$$\frac{d}{dt}\nabla^2 \Phi = \alpha(\Phi - \Phi_B) - \frac{\beta}{n}\frac{\partial n}{\partial y} \tag{7}$$

The mechanism for convective transport of blobs, is that the curvature term ($\propto q$ or β) in Eqs. (6) or (7) drives an electrostatic potential Φ with y variation, and hence gives rise to a velocity $v_x = -\partial\Phi/\partial y$.

In the remained of the paper we specialize to the class of solutions with aligned density and temperature contours, and for simplicity consider the case T(n) = n. Thus only one of Eqs. (2) and (3) need to be time advanced.

Solutions for the various limits of these equations indicated will be explored in the next section.

III. Results

We begin by exploring the difference in blob propagation in the thermalized and hot blob models., viz. Eq. (6) with T = constant and T(n) = n, first considering the non-spinning $\Phi_B = 0$ limit. In the hot blob model with T(n) = n, and momentarily dropping the a_s term for simplicity, the curvature-induced potential is

$$\Phi = 2qn^{1/2}\frac{\partial n}{\partial y} \tag{8}$$

which is to be compared with the result in the thermalized limit T = 1

$$\Phi = \frac{q}{n}\frac{\partial n}{\partial y} \tag{9}$$

Because of the $n^{1/2}$ vs. n^{-1} weightings of $\partial n/\partial y$, the hot blob model gives a larger Φ and hence a larger velocity to the high density region near the blob maximum, while slowing the low density extremities of the blob. In the absence of blob instabilities, a thermalized blob propagates as a coherent object (i.e. it maintains a relatively fixed or slowly evolving shape in its own moving reference frame), but a hot blob develops strong fingering or a radial streamer structure.

Numerical results comparing these case are shown in Fig. 1. The blobs were initialized at t = 0 with a Gaussian density profile

$$n(r) = \exp(-r^2/2a^2) + n_f \tag{10}$$

and allowed to evolve under Eqs. (2) and (6). Parameters for this comparison are $a = 10$, $q = 2.5$, $a_s = 5$ and $n_f = 0.01$. To improve the quality of the numerical runs and avoid noise at the scale of the grid, a small diffusion term was added to Eq. (2), with D = 0.002 for these runs. For the thermalized blob case of Fig. 1 (a) we took T = constant = 0.57, choosing the numerical value of T for convenience [i.e. to make the final state at t = 2250 fit on the same frame as the other cases in parts b) and c)] noting from Eq. (2) that Φ, and the resulting blob velocity scale with $qT^{3/2}$ in this case. Although the thermalized blob equations permit an exact analytical solution[7,8] (i.e. a Gaussian in a frame moving with velocity $u_x = q/a^2$) for these parameters, the blob is unstable[15,16] and is beginning to break up along its leading edge. Turning to Fig 1 b), a finger or streamer is clearly seen in the hot blob result. This finger can be considered as a nonlinear limit of the same curvature-driven instability, enhanced by the weighting discussed above in Eqs. (8) and (9).

Fingers are prominent when $a_s < a$, as in the example of Fig 1 b). In the opposite limit $a_s > a$ (not shown) the term involving ∇^2 in Eq. (6) dominates the determination of the potential. Inversion of this operator smoothes the spatial structure of Φ and results in density evolution contours that are more reminiscent of a mushroom shape,[14] rather than a sharp finger.

Spin dramatically alters the results, as can be seen in Fig. 1 c) where we solve the hot blob Eq. (6) with the same parameters, except that now we consider the strongly spinning case $\Phi_{B0} = 5$. First we note that spin stabilizes the curvature-driven instabilities and suppresses the development of fingers. Spin convects perturbations through both the "bad" and "good" curvature sides of the blob mitigating instability. Furthermore, the flow pattern due to spin is necessarily sheared for any confined T(r) profile, and this shearing provides additional stabilization of curvature-driven modes. However, a spinning blob may become unstable to rotational instabilities. These are being addressed in a separate publication.[17]

Although Eqs. (2) and (6) are already dimensionless (to the scales set by Ω_i and ρ_s) a further scaling invariance of this system is apparent, and motivates normalizing space scales to a and time scales to the spin time $\tau_s = a^2/\Phi_{B0}$. The resulting equations contain only two parameters: a_s^2 / a^2 and $\varepsilon \equiv 2q/a\Phi_{B0}$. For small ε, the blob is rapidly spinning, curvature imposes a small perturbation on the evolution of the system, and the lowest order density and potential are functions of r alone. For larger ε (i.e. weaker spin), the blob begins to leave a trailing wake behind as it propagates. An extreme case is illustrated in Fig. 2 with $\varepsilon = 0.4$. [This corresponds to the same parameters as in Fig. 1 c) except that q = 10.] Here, and all figures of this paper, the spin is *clockwise*. The comet-like tail forms because the blob leaves a trailing wake which is then spun around and left behind as the blob propagates. [The lower density wake is left behind because of the $n^{3/2}$ scaling of velocity implied by Eq. (8)] Convective curvature-driven instability on the bad curvature (large x) side of the blob appears to be ejecting a plasma perturbation which would reach maximum amplitude at the bottom of the blob for clockwise spin. The differential spin, being more rapid at smaller r, results in the observed pattern. This explanation is more evident from movies than from the still frame shown here.

The figure illustrates a downward motion in y of the blob which can be understood as follows. Examine $\partial n/\partial y$ along the line $y = y_0$ where (x_0, y_0) is the density maximum. In the wake, $x < x_0$, $\partial n/\partial y > 0$ because of the ejected material in the comet-like tail. At the center, $x = x_0$, $\partial n/\partial y = 0$ by definition of the maximum. Thus $\partial/\partial x$ $(\partial n/\partial y) \propto \partial\Phi/\partial x = v_y < 0$. Our earlier spin-less theories of blob propagation have provided a mechanism for v_x but not v_y (except of course for a uniform E × B drift in a background potential). The preceding discussion provides one candidate explanation of the more complicated poloidal and radial motion that is sometimes observed in simulations and imaging experiments. A second mechanism for v_y will be discussed later.

So far we have only considered the solutions of the vorticity equation in the dissipative limit given by Eq. (6). This has allowed an investigation of the role of the spin through the convective nonlinearity $\mathbf{v}\cdot\nabla n$. It has been shown that this nonlinearity mitigates asymmetries in density. This profoundly affects the blob dynamics but only influences the polarization-induced charge indirectly.

Next we investigate the hydrodynamic case given by Eq. (7) which contains the $\mathbf{v}\cdot\nabla\nabla^2\,\Phi$ nonlinearity, viz. the convection of vorticity or charge. For this investigation, a code described in Ref. 16 has been employed with the addition of spin through $\Phi_B = \Phi_{B0}T$ with $T = n$. Results for the scaled x-velocity of blob propagation are shown in Fig. 3. When both the spin and vorticity convection term are neglected, the analytical model of Ref. 8 applies, the blob velocity has the simple scaling $v_x = q/a^2$ and results in a characteristic time for a blob to convect one blob radius of $\tau_c = a^3/q$. This scaling leads to straight-line trajectories in Fig. 3. For the non-spinning cases, comparing $a = 30$ and $a = 10$, the results show that the speed increase with smaller a is not quite proportional to $1/a^2$ as embodied in the analytical scaling. Rather there is a weaker dependence because of the importance of the vorticity convection term $(\mathbf{v}\cdot\nabla\nabla^2\Phi > \alpha\Phi)$ at small a.[16] Comparing the spinning and non-spinning blobs for the same a, spinning blobs move more slowly than their non-spinning counterparts. Finally note that all blobs move at the same speed for $t \ll \tau_c, \tau_s$ because there is not time for charge mixing by vorticity convection due to Kelvin-Helmholtz (KH) instability[16] or spin. For the parameters of the figure, the scaled spin time $\tau_s/2\tau_c$ is 0.11 for $a = 10$ and 0.04 for $a = 30$.

The simulations employed to obtain Fig. 3 exhibit a rich variety of phenomena. At longer times than shown in the figure, there are significant ambiguities in the blob trajectories due to blob instabilities which distort the blob's shape, and in extreme cases, which destroy its coherence. As noted previously, the curvature-driven and KH instabilities are present for non-spinning blobs. In the spinning case, rotational instabilities with an azimuthal mode number of 2 are observed.[17] These instabilities result in a pinwheel pattern (somewhat resembling a spiral galaxy) that ejects the outer region of the blob. A discussion of rotational instabilities and more detailed results of these simulations will be presented elsewhere.[17] A second point of interest from these simulation results is that the blobs typically show motion in both x and y directions. The mechanism for the slowing of v_x and the generation of v_y will be presented next.

In situations for which the blob maintains coherency for many spin and convection times it is possible to understand the dynamics of the bulk blob propagation from a simple analytical model based on the physics of charge mixing that was discussed in the introduction. We begin from Eq. (7) by transforming to the blob frame, which is translating with constant velocity $\mathbf{u}$ as yet undetermined. Let

$$\Phi = \Phi_B(r) + \phi(r,\theta) \tag{11}$$

and also consider $n = n(r)$ on the RHS of Eq. (7). The basic ordering is that $\Phi_B \sim 1$, $\nabla \sim 1/a$, where a is the blob radius in units of ρ_s ($a \gg 1$), and $\alpha \sim \beta \sim 1/a^4$. From this we see that $\phi \sim 1/a \ll \Phi_B$. Linearizing the convective derivative term for $\phi \ll \Phi_B$, dropping order ϕ^2 and noting that $\mathbf{b}\times\nabla\Phi_B \cdot\nabla^2\Phi_B = 0$, Eq. (7) becomes, in the blob frame

$$(\mathbf{v}_\phi - \mathbf{u})\cdot\nabla\nabla^2\Phi_B + \Omega\frac{\partial}{\partial\theta}\nabla^2\phi - \alpha\phi = -\frac{\beta}{n}\frac{\partial n}{\partial y} \tag{12}$$

where $\mathbf{v}_\phi = \mathbf{b} \times \nabla\phi$ is associated with the blob convection due to charge polarization and $\mathbf{v}_B = \mathbf{b} \times \nabla\Phi_B$ is associated with the spin. Here, we have set $\mathbf{v}_B \cdot \nabla = \Omega \, \partial/\partial\theta$ where $\Omega = r^{-1} \, \partial\Phi_B/\partial r$, and also Eq. (12) presumes a solution that is steady-state in the blob frame. We note that the assumption $\mathbf{v}_\phi \cdot \nabla\nabla^2\phi \ll \alpha\phi$ requires $\phi \ll \alpha a^4$, or assuming $\phi \sim q/a$, $a \gg a_* \equiv (q/\alpha)^{1/5}$. The scale a_* is the fundamental dimensionless blob scale in the absence of spin and dissipation.

To illustrate the physics, we simplify by considering the rigid rotor case, $\Omega =$ const. When blob spin is due to sheaths, this cannot happen for a blob with a confined $T(r)$ profile, but here the rigid rotor assumption is actually only needed in the vicinity of the polarization charge which creates the velocity shear $\mathbf{v}_\phi - \mathbf{u}$. In the rigid rotor limit we have $\Phi_B = \Omega r^2/2$, $\nabla^2\Phi_B = 2\Omega$ and $\nabla\nabla^2\Phi_B = 0$, thus the equation to be solved is

$$\Omega \frac{\partial}{\partial\theta} \nabla^2\phi - \alpha\phi = -\frac{\beta}{n} \frac{\partial n}{\partial r} \sin\theta \tag{13}$$

Although it is simple to construct a general solution to Eq. (6), the most insight is gained by the small and large α limits. Comparing the terms on the LHS of Eq. (6), the expansion parameter is seen to be $W = \Omega/(\alpha a^2)$ which is the ratio of charge transport by spin to parallel charge loss to the sheaths. For $W \gg 1$ we obtain

$$\Omega \frac{\partial}{\partial\theta} \nabla^2\phi = -\frac{\beta}{n} \frac{\partial n}{\partial r} \sin\theta \tag{14}$$

It can be seen that

$$\phi = \phi_c(r)\cos\theta \tag{15}$$

This induced potential will cause an E×B drift that controls the blob's translation motion according to

$$v_y = \frac{\partial\phi}{\partial x} = \cos\theta \frac{\partial\phi}{\partial r} - \frac{\sin\theta}{r} \frac{\partial\phi}{\partial\theta} \tag{16}$$

$$v_x = -\frac{\partial\phi}{\partial y} = -\sin\theta \frac{\partial\phi}{\partial r} - \frac{\cos\theta}{r} \frac{\partial\phi}{\partial\theta} \tag{17}$$

Using Eq. (15) and averaging over θ

$$\langle v_x \rangle = 0 \tag{18}$$

$$\langle v_y \rangle = \frac{1}{2} \frac{\partial\phi_c}{\partial r} + \frac{1}{2r}\phi_c = \frac{1}{2r} \frac{\partial}{\partial r}(r\phi_c) \tag{19}$$

where from Eq. (14) we estimate

$$\phi_c = \left(\Omega\nabla_*^2\right)^{-1} \frac{\beta}{n} \frac{\partial n}{\partial r} \sim \frac{q}{Wa} \tag{20}$$

8

where $\nabla_*^2 = \nabla^2 - 1/r^2$ i.e. $\nabla^2[\phi(r)\cos\theta] = \cos\theta\nabla_*^2\phi(r)$.

In the opposite limit $W << 1$ we can neglect Ω to lowest order in Eq. (13) to obtain

$$\phi = \phi_s(r)\sin\theta \tag{21}$$

$$\phi_s = -\frac{q}{n}\frac{\partial n}{\partial r} \tag{22}$$

To this order one obtains the usual estimate for the blob velocity without spin, viz.

$$\langle v_x \rangle = -\frac{1}{2r}\frac{\partial}{\partial r}(r\phi_s) \tag{23}$$

$$\langle v_y \rangle = 0 \tag{24}$$

which implies $v_x \sim q/a^2$. The effect of Ω is then determined by higher order expansions. Iterating on Eq. (13) by using the lowest order solution, Eq. (21) in $(\Omega/\alpha)(\partial/\partial\theta)\nabla^2\phi$ we obtain, through order W^2

$$\phi = \left(1 - \frac{\Omega^2}{\alpha^2}\nabla^4 + ...\right)\frac{q}{n}\frac{\partial n}{\partial r}\sin\theta + \left(\frac{\Omega}{\alpha}\nabla^2\frac{q}{n}\frac{\partial n}{\partial r} + ...\right)\cos\theta \tag{25}$$

This shows a reduction in v_x and the development of v_y as the parameter W is increased.

In summary, $W = \Omega/(\alpha a^2)$ is the fundamental parameter that controls the velocity slowdown by spin. For $W << 1$ spin is ineffective and $v_x \sim q/a^2$. As W increases, we get a reduction in v_x and the development of v_y. For $W \sim 1$ we expect $v_x \sim v_y$. For $W >> 1$ we find $v_x = 0$ (to order $1/W$) while $v_y \sim q/Wa^2$. In this large spin limit, the charge polarization mechanism results in primarily poloidal rather than radial blob motion.

In order of magnitude $\Omega \sim \Phi_B/a^2$, but it is worth noting that for a Gaussian blob on a low density background, most of the induced charge occurs at $r >> a$ (recall that $\nabla^2\phi \equiv 0$ for the vacuum case). Consequently the local value of Ω can be exponentially smaller than Φ_B/a^2.

The preceding simple model is approximate because it neglects the complexities caused by instabilities and blob mass loss that are seen in the simulation, but it qualitatively describes the phenomena of the suppression of v_x and the generation of v_y due to spin-induced charge mixing. Comparing with the simulations of Fig. 3, the model works well for the $a = 10$ case, predicting the observed factor-of-two slowdown in v_x. For the $a = 30$ case, the model predicts negligible slowdown. We speculate that the slowdown seen in the simulations for $a = 30$ is not the result of charge mixing but rather the result of the convective term $\mathbf{v} \cdot \nabla n$ stabilizing the curvature instability (which is responsible for the apparent acceleration seen in the upper curve of Fig. 3). This stabilization mechanism is the same one that was demonstrated in Fig. 1.

The remainder of this section will be devoted to studying the effects of an externally imposed sheared velocity field $V_y(x)$ on the motion of blobs. A blob in the SOL is naturally exposed to a sheared velocity field because it $\mathbf{E} \times \mathbf{B}$ drifts in the SOL electric field $E_x = -\Phi_{B0} \, \partial T_e/\partial x$ from the Bohm sheath potential due to the background temperature profile.

Subtracting off a constant mean poloidal velocity, which is ignorable for the blob dynamics, we add a pure shear flow field by the replacement in Eq. (6)

$$\Phi_B \rightarrow \Phi_{B0} T(n) + \Phi_{x0}(x/a)^2 \tag{26}$$

For a $T_e(x)$ profile that decays exponentially in the SOL, the resulting shear coefficient Φ_{x0} ($\propto \partial^2 T/\partial x^2$ at the blob center) is positive and corresponds to an external shear that opposes the spin of the blob. We refer to this case as counter-shear. Conversely, negative Φ_{x0} implies co-shear. Note that when $\Phi_{x0} < \Phi_{B0}$, Eq. (26) implies that the external shear flow at one blob radii $x \sim r \sim a$ is small compared with the blob spin.

In Fig. 4 we again launch a Gaussian blob from the origin at t = 0 and follow its evolution up to t = 4000 for a) co-shear, b) counter- shear and c) non-spinning cases. Parameters are the same as for Fig. 1 c) and $\Phi_{x0} \ll 1$ is given in the caption. Comparing 4 a) or b) with 4 c) we conclude that spin dramatically increases the coherency of the blob and allows coherent blob propagation even in the presence of external sheared flows that completely smear out and destroy the fingers (streamers) in c).

In the non-spinning case 4 c) where we solve the hot blob equations [Eqs. (2) and (6) with T(n) = n and $\Phi_{B0} = 0$], the external sheared flow strongly inhibits transport in the x direction. The periodicity in y of the simulation, which models the interaction of adjacent fingers [see the finger without external sheared flows in Fig. 1 b)], leads to the observed mixing as the shearing progresses. In the presence of dissipation (D and a_s) the time-asymptotic state is uniform in y and hence non-propagating in x. This transport inhibition of streamers by sheared flows is akin to well known results.

In contrast, externally sheared flows do not destroy the blob coherency in the spinning cases, 4 a) and b) because in these cases the external sheared flows are weak compared with the blob spin, i.e. $\Phi_{x0} \ll \Phi_{B0}$. The spin prevents the development of fingers, keeping each blob localized (and non-interacting with any neighbors).

Comparing these two spinning cases in more detail, for the counter-shear case, corresponding to a "normal" decaying $T_e(x)$ background profile, a slight *increase* in the blob's x-velocity occurs due to the sheared flow, while a slight decrease results in the co-shear case. The changes in speed $\propto \partial n/\partial y$ are consistent with the observed elongations of the blob in x and y for the counter and co cases respectively. It should be noted that spinning blobs are subject to charge-induced mixing when $\Omega/\alpha a^2 > 1$ as discussed following Eq. (25). The role of external sheared flows in this regime remains to be investigated.

The differences in convective velocity that we have been considering are illustrated more dramatically in Fig. 5 which shows the time evolution of the position of the center of mass of the plasma (initiated as a Gaussian blob) for five comparative cases. The most rapid transport occurs in the case without spin or external sheared flow and the smallest transport occurs in the case that has external sheared flow without spin. The effect of shear (Φ_{x0}) on the velocity of a spinning blob is not linear, and shows asymmetries with respect to sign. The evolution of the counter-sheared case is very sensitive to Φ_{x0} (which is why such a small value was chosen). This sensitivity is probably a consequence of the fact that the external sheared flow combines with the spin to give a stagnation point.

The present results for the interaction of hot blobs with external sheared flows can be compared with the results of similar studies for *thermalized* blobs, i.e. T(n) = constant. In Appendix A of Ref. 8 it was shown that the coherency and blob velocity v_x of large ($a \gg a_s, a_*$) thermalized blobs propagating through weak shear layers are not much affected by external sheared flows. In Ref. 16, however it was shown that for $a \sim a_*$ and (in the present notation) $\Phi_{x0} > \Phi_{x0}^{crit} \equiv (q/a)(a/a_*)^5$ strong deformation and some loss of coherency of the blob occurs as it passes through a localized sheared layer. In general, loss of coherency is to be expected whenever the nonlinearities in the $(d/dt)\nabla^2\Phi$ term become significant, since this term is associated with the mode coupling and energy/vorticity cascades of hydrodynamic turbulence.

IV. Discussion and Conclusions

In this paper we have extended the theory of convective transport in the SOL by blobs to include the effects of electron energy as well as density transport. This generalization requires the consideration of an internal temperature profile within the blob and leads naturally to internal blob spin when the blob is connected in the parallel direction to sheaths. Both spinning and non-spinning solutions of the hot blob equations have been investigated.

The main conclusions from this study are as follows. While the thermalized blob equations that were considered previously have an exact solution that convects an isolated density blob in a vacuum without distortion, the hot blob equations without spin typically result in plasma fingers (also referred to in the literature as fronts or streamers) and mushrooms that propagate forward at a rapid velocity while leaving behind a pronounced wake.

Blob spin, normally present when the blobs connect to sheaths in the parallel direction, introduces several important effects; (i) the blob coherence and symmetry are increased, (ii) the blob radial (i.e. in the direction $\mathbf{e}_x = \mathbf{R}/R$) velocity is slowed, and (iii) two mechanisms for poloidal motion (i.e. in the direction $\mathbf{e}_y = \mathbf{b} \times \mathbf{e}_x$) of the blob are introduced. Both the spin-induced convection of density $\mathbf{v}\cdot\nabla n$ and of charge $\mathbf{v}\cdot\nabla \nabla^2\phi$ play a role in these phenomena. It was shown by a relatively simple analytical model

that an important mechanism for the velocity dependence on spin is the spin-induced mixing of the curvature-generated charge separation. Coherency of the blob against internal curvature instabilities is enhanced by the spin; but, the blob may become unstable to rotational instabilities when $\Phi_{B0}/\alpha a^4 \gg 1$.[17]

Finally, the effect of externally imposed sheared-flows on convective transport was considered. This complements previous work done on the effect of sheared flows on thermalized non-spinning blobs.[8,16] It was shown that while external poloidal velocity shear inhibits radial transport in the case of non-spinning fingers (i.e. radial streamers) through shearing-induced interactions with poloidally adjacent neighbors, for spinning blobs the interaction of the blob with the external velocity field depends on the sign of the external shear with respect to the spin. Importantly, for large blobs ($a > a_*$) spin permits the blob to pass coherently through a shear layer which would break up a non-spinning finger.

In conclusion, hot blobs that are sheath-connected and hence spinning are not as effective at either energy or particle transport as non-spinning blobs. Since spin is a natural consequence of sheath physics, this motivates further work into the conditions for parallel sheath connection and the behavior of blobs in the disconnected limit. It is anticipated from the present results (where disconnection was modeled by artificial spin suppression) that a complete theory of disconnected blobs will show enhanced convective transport when compared with their connected, spinning counterparts. If so, the roles of parallel connection and the presence or absence of spin may have significant implications for understanding the density limit. In turbulence simulations relevant to the density limit[18] it has been shown that rapid perpendicular energy transport, and concomitant cooling of the edge T_e, acts synergistically with disconnection physics and increased resistivity at low T_e. The relationship of this observation to fundamental blob physics merits further study.

Finally, we end with the caveat that the present paper has only explored the class of solutions with $T = T(n)$. Even though n and T obey identical advection equations, Eqs. (2) and (3), for time-scales $t < \tau_{E\parallel}$, more general solutions are possible, and may be of interest in understanding recent simulation results.[19]

References

1 M. Umansky, S. I. Krasheninnikov, B. LaBombard and J. L. Terry, Phys. Plasmas 5, 3373 (1998); B. LaBombard, M. V. Umansky, R. L. Boivin et al., Nucl. Fusion 40, 2041 (2000); B. LaBombard, R. L. Boivin, M. Greenwald et al., Phys. Plasmas 8, 2107 (2001).

2 S. J. Zweben, R. J. Maqueda, D. P. Stotler *et al.*, Nucl. Fusion **44**, 134 (2004).

3 G. Y. Antar, G. Counsell, Y. Yu, B. LaBombard, and P. Devynck, Phys. Plasmas **10**, 419 (2001).

4 J. A. Boedo, D. Rudakov, R. Moyer *et al.*, Phys. Plasmas **8**, 4826 (2001); D. Rudakov, J. Boedo, R. Moyer *et al.*, Plasma Phys. Control. Fusion **44**, 717 (2002).

5 Å. Fredriksen, C. Riccardi, L. Cartegni and H Pécseli, Plasma Phys. Control. Fusion **45**, 721 (2003).

6 A. Yu. Pigarov, S. I. Krasheninnikov, T. D. Rognlien, M. J. Schaffer, and W. P. West, Phys. Plasmas **9**, 1287 (2002).

7 S. I. Krasheninnikov, Phys. Lett. A **283**, 368 (2001).

8 D. A. D'Ippolito, J. R. Myra, and S. I. Krasheninnikov, Phys. Plasmas **9**, 222 (2002).

9 N. Bian, S. Benkadda, J-V. Paulsen, and O. E. Garcia, Phys. Plasmas **10**, 671 (2003).

10 O. E. Garcia, N. H. Bian, J.-V. Paulsen, S. Benkadd and K Rypdal, Plasma Phys. Control. Fusion **45**, 919 (2003).

11 Y. Sarazin, Ph. Ghendrih, G. Attuel, *et al.*, J. Nucl. Mater. **313-316**, 796 (2003).

12 P. B. Parks, W. D. Sessions, and L. R. Baylor, Phys. Plasmas **7**, 1968 (2000).

13 D.A. D' Ippolito, J.R. Myra, S.I. Krasheninnikov, G.Q. Yu and A.Yu. Pigarov, invited paper, 9th International Workshop on Plasma Edge Theory in Fusion Devices, San Diego CA, 3 – 5 September 2003, to be published in Contrib. Plasma Phys.

14 S. I. Krasheninnikov, D. D. Ryutov, and G. Q. Yu, Invited Paper, International Toki Conference, to be published in Journal of Plasma and Fusion Research (2004).

15 D.A. D' Ippolito and J.R. Myra, Phys. Plasmas **10**, 4029 (2003).

16 G. Q. Yu and S. I. Krasheninnikov, Phys. Plasmas **10**, 4413 (2003).

17 D. A. D' Ippolito, J. R. Myra, D. A. Russell, G. Q. Yu and S. I. Krasheninnikov, private communication (2003); (to be submitted to Phys. Plasmas)

18 X. Q. Xu, W. M. Nevins, T. D. Rognlien, *et al.*, Phys. Plasmas **10**, 1773 (2003).

19 D. A. Russell, J. R. Myra, D. A. D' Ippolito, W. M. Nevins and X. Q. Xu, Bull. Am. Phys. Soc **48**, 226 (2003), poster LP1.071.
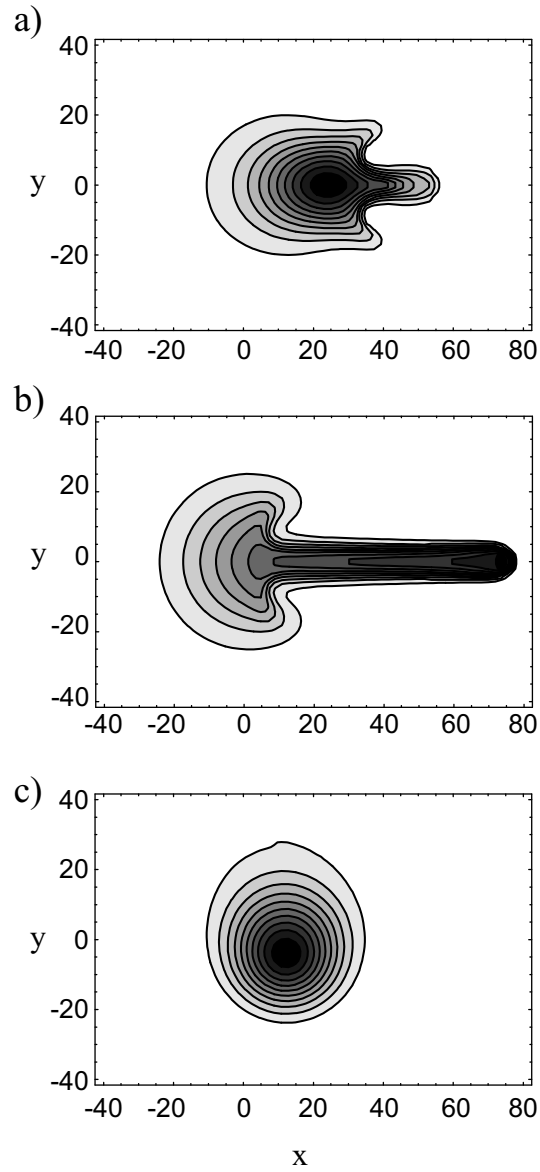
Fig 1. Density contours at t = 2250 of a blob that was released at t = 0 as a circular Gaussian with center at x = y = 0: a) thermalized density blob with T = constant ($\Phi_{B0} = 0$), b) same case for a hot but non-spinning blob with T(n) = n ($\Phi_{B0} = 0$), and c) hot spinning blob ($\Phi_{B0} = 5$). Units are normalized to Ω_i and ρ_s. Note that spin provides coherency by suppressing the curvature-induced instability seen in a) and the fingering seen in b). Comparing b) and c), spin reduces the radial convection of the blob maximum.
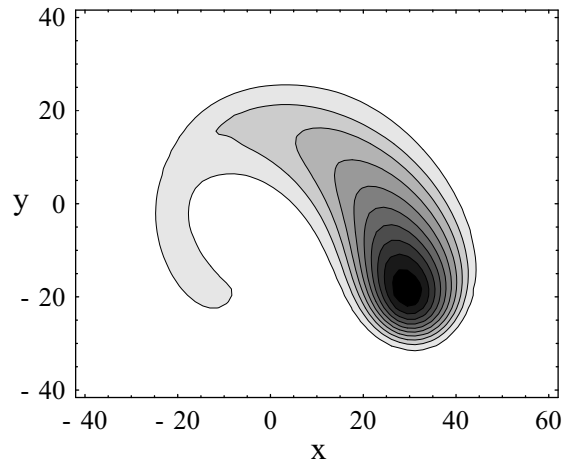
Fig 2. Weakly spinning blob ($2q/a\Phi_{B0} = 0.4$) at t = 1000 showing the development of a comet-like tail which arises from the wake in the presence of spin. Note the y-displacement of the center from the launch point at x = y = 0, indicating motion in both radial (x) and poloidal (y) directions even though the curvature "force" is entirely radial.

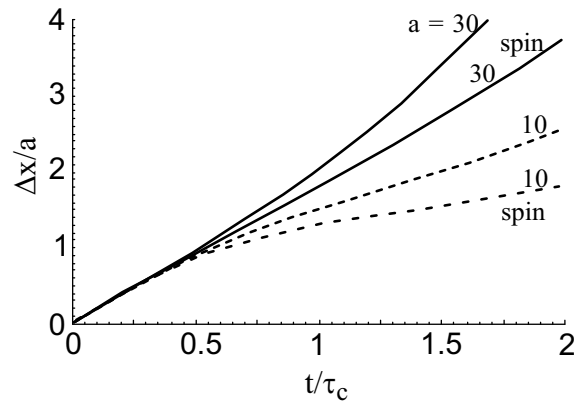Fig 3. Normalized radial displacement Δx of blob maximum vs. time normalized to blob convection time τ_c = a^3/q. Numbers indicate the value of a. The curves labeled "spin" have Φ_{B0} = 10, while the curves without the "spin" label have Φ_{B0} = 0. Note that (i) the speed increase as $a \rightarrow 0$ reflected in the scaling of τ_c is saturated by the vorticity convection term, (ii) for the same a, spinning blobs move more slowly than their non-spinning counterparts, and (iii) that all blobs move at the same speed for t $\ll \tau_c$, τ_s where the spin time is τ_s = a^2/Φ_{B0} because there is not time for charge mixing by vorticity convection due to KH instability or spin.
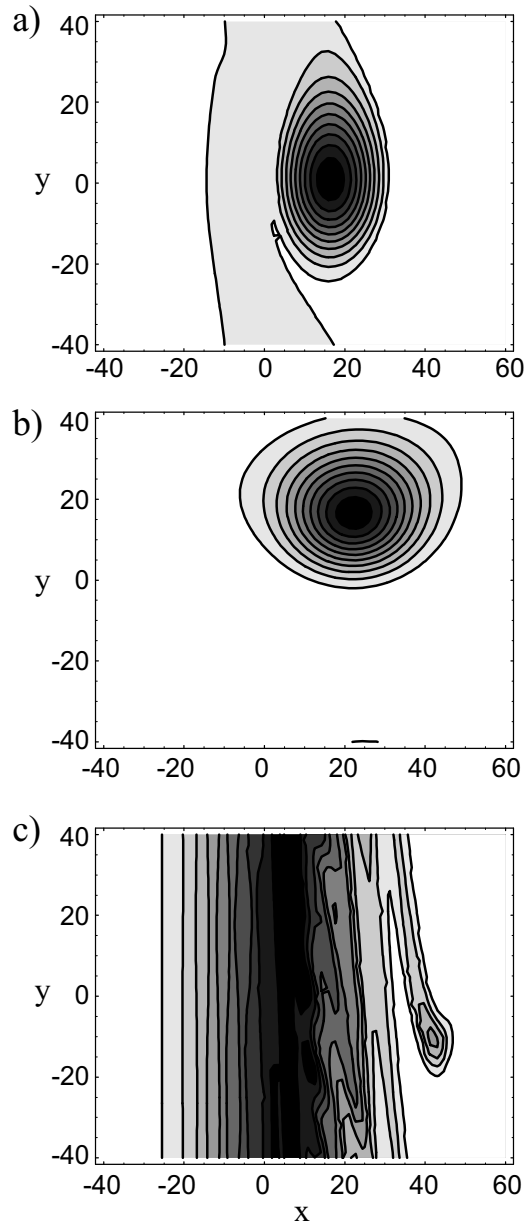
Fig 4. Effect of external sheared flows on blob evolution. Shown above are density contours at t = 4000 of a blob that was released from the origin at t = 0 as a circular Gaussian: a) a spinning blob in a strongly co-sheared flow ($\Phi_{x0} = -0.2$, $\Phi_{B0} = 5$), b) a spinning blob in a weakly counter-sheared flow ($\Phi_{x0} = 0.02$, $\Phi_{B0} = 5$), c) final state of a non-spinning blob for the same parameters and time as in a) but with $\Phi_{B0} = 0$.
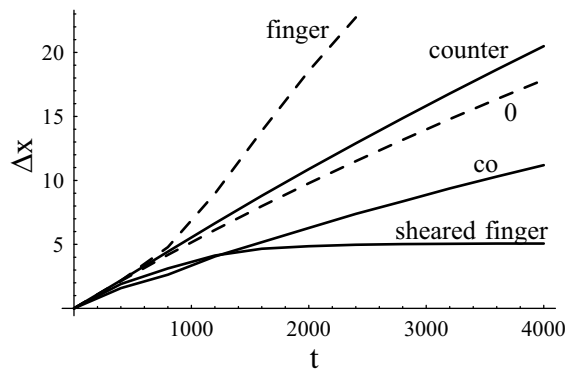
Fig 5. Center of mass transport (radial position vs. time) for five comparative cases showing the effect of external sheared flows and spin. Cases with no external sheared flows are shown with a dashed curve. "Finger" is the non-spinning hot blob case of Fig 1 b) in the absence of external shear and "sheared finger" is the same case with external sheared flow [i.e. the case of Fig. 4 c)]. Note that sheared flow strongly inhibits transport. "Co", "0" and "counter" refer to spinning blob cases. "Co" is the co-shear case of Fig. 4 a). "Counter" is the counter-shear case of Fig. 4 b). "0" is the case of a spinning blob with no external shear shown in Fig. 1c). For these spinning blob cases, the effect of sheared flow depends on the sign of the shear with respect to the spin.